BirEx JOURNAL
Budapest International Research in Exact Sciences
Medical, Biological, Argiculture, Engineering
Science and other related areas
e-ISSN : 2655-7827
p-ISSN : 2655-7835
http://www.bircu-journal.com/index.php/birex

Mineralogical determination of Bemololo, Miandrivazo and Analavory clays by X-ray diffraction for applications

Ramahandry Jean Elidon[1], Robijaona Rahelivololoniaina Baholy[1,2], Randriantsimbazafy Andrianirina[3], Razafindramanga Athou Wega[1], Letsara Rokiman[1,4], Rabearisoa Solotiana Rija[1], Koto-te-Nyiwa Ngbolua[5,6], Mandimbiiharison Aurélien[7]

[1]*Industrial, Agricultural and Food Process and Systems Engineering, Ecole Supérieure polytechnique d'Antananarivo, University of Antananarivo, Antananarivo, Madagascar*
[2]*Laboratory for the Valorization of Natural Resources, Polytechnic High School of Antananarivo, Madagascar*
[3]*Ecole Supérieure Polytechnique d'Antananarivo, University of Antananarivo, Antananarivo, Madagascar*
[4]*Tsimbazaza Zoological and Botanical Park - Antananarivo, Madagascar*
[5]*Department of Biology, Faculty of Science, University of Kinshasa, Kinshasa, Democratic Republic of the Congo*
[6]*Department of Environmental Sciences, Faculty of Science, University of Gbado -Lite, Gbado-Lite, Democratic Republic of the Congo*
[7]*École Supérieure Polytechnique d'Antananarivo, Geology Department, University of Antananarivo, Antananarivo, Madagascar.*
Corresponding author: baholy.robijaona@univ-antananarivo.mg

Abstract: *After characterizing the clay minerals from the Bemololo (BMLL), Miandrivazo (MNDV), and Analavory (ANLV) deposits using X-ray diffraction (XRD), dye absorption experiments and photochemical screening analyses were conducted to determine the potential applications for each clay. XRD analysis revealed that the Bemololo deposit comprises the following mineral compositions: BMLL 001 is rich in muscovite; BMLL 002 contains a mixture of vermiculite, sepiolite, and amphibole; BMLL 003 is composed of kaolinite and chlorite; and BMLL 004 is predominantly kaolinite. For the Miandrivazo deposit, MNDV 001 is a mixture of kaolinite, muscovite, and chlorite; MNDV 002 contains chlorite and muscovite; and MNDV 003 comprises kaolinite and muscovite. The Analavory deposit features ANLV 001, which contains aragonite and calcite, and ANLV 002, identified as vermiculite clay. Dye absorption experiments indicated that BMLL 001, BMLL 002, and BMLL 003 have potential applications in water treatment, particularly in the removal of unwanted dyes or ions. Additionally, photochemical screening revealed the presence of deoxyose in BMLL 004, while BMLL 002, ANLV 002, and ANLV 001 were found to contain tannins.*
Keywords: *clays; X-ray diffraction; adsorption; and photochemical screening.*

I. Introduction

Clays are naturally abundant materials that have been used for centuries due to their versatile properties and many industrial applications. However, despite their widespread use, particularly in Madagascar, there still needs to be a significant gap in understanding the specific mineralogical and physicochemical properties of different types of clay. This shortcoming limits the optimization of their potential applications. In Madagascar, clays from the Bemololo, Miandrivazo, and Analavory regions are commonly used in local industries, including cosmetics, pharmaceuticals, and pottery, often based on traditional knowledge rather than rigorous scientific characterization. Previous research has focused on the general properties of clays and their applications based on their mineral content, particle size distribution, and chemical composition. Work by Grim (1968), Moore and Reynolds (1989),

as well as more recent research by Bergaya and Lagaly (2013), has laid the foundation for understanding the general applications of clays. However, these studies need to pay more attention to localized varieties such as those from Madagascar. Although some research has been carried out on Analavory yellow clay for its use in cosmetics and pharmacy (Abdoulkader et al., 2021), data complete mineralogical records for the clays of Bemololo and Miandrivazo remain rare.

Additionally, existing studies often need more detailed X-ray diffraction (XRD) analyses, which are essential for accurately identifying mineral phases present in clays. This study is notable for its focus on a detailed mineralogical determination of the Bemololo, Miandrivazo, and Analavory clays using XRD analysis, aiming to provide a deeper understanding of the mineral composition and structure of these clays, which is little documented in the existing literature. The results of this mineralogical characterization could have a significant impact on various industries, notably by improving the quality control of clay-based products and optimizing their use in cosmetics, pharmaceuticals, and even construction as a component of ceramics and bricks. A better understanding of mineralogical composition can also promote the development of new applications, such as environmental remediation technologies using clays as pollutant adsorbents or the creation of catalysts for chemical processes. This study thus aims to carry out a comprehensive mineralogical analysis of Bemololo, Miandrivazo, and Analavory clays by X-ray diffraction, providing essential information that will support their optimal application in various industrial sectors.

II. Material and Methods

2.1 Plant Materials

a. Sample source

The clay samples analyzed in this study were collected from three distinct locations: Analavory, Bemololo, and Miandrivazo, as outlined in Table 1 below. A total of nine samples were obtained, with one sample per collection site sent to the laboratory for Analysis. The mineralogical characterization of these samples was conducted using X-ray diffraction at the Laboratoire de Géologie des Argiles in Liège.

Table 1. Clay samples used in this study

Location	Sample coding	Laborde contact details	Altitude	Color
Bemololo	BMLL 001	X= 467 843m Y= 699 631m	1601m	Green clay
	BMLL 002	X= 467 970m Y =699 748m	1621m	White clay
	BMLL 003	X= 467 978m Y= 699 743m	1623m	Greyish clay
	BMLL 004	X= 468 063m Y= 699 757m	1619m	Violet clay
Miandrivazo	MNDV 001	X= 296 426m Y= 727 533m	64m	Green clay
	MNDV 002	X= 296 546m Y= 727 813m	69m	Orange green clay
	MNDV 003	X= 296 559m Y =727 774m	71m	Red clay
Analavory	ANLV 001	X= 797 203m Y= 421 353m	951m	Yellow clay
	ANLV 002	X= 797 065m Y =421 388m	949m	Green clay

BLLM, MNDV, and ALV are the codes for samples taken from Bemololo, Miandrivazo, and Analavory, respectively, with 'm' denoting meters.

b. Sample preparation prior to XRD analysis

Sample preparation adhered to the protocol established by the Clay, Geochemistry, and Sedimentary Environments Laboratory at the University of Liège, which was adapted from **Moore** and **Reynolds**'s (**1989**) methodology. Both the total powder and the clay fraction were subjected to this preparation process.

Total powder

The preparation involved several sequential steps. Initially, the samples were dried in an oven at 40°C for a minimum of 48 hours. Following drying, the samples were ground using an agate mortar. The ground material was then sieved through a 250 µm sieve to isolate particles smaller than this threshold. Finally, the resulting fine powder was pressed into pellets using metal supports, rendering them suitable for subsequent Analysis.

Clay fraction

A small quantity of the dried sample is placed in a beaker, to which distilled water is added. The mixture is stirred using a magnetic stirrer equipped with a bar magnet until homogeneity is achieved. Once the mixture is uniform, it is sieved through a 63 µm sieve, with additional distilled water added during the sieving process. The fraction passing through the sieve is collected in a flask, where more distilled water is added. After vigorous shaking, the flask is allowed to settle for 50 minutes. The clay fraction, comprising particles smaller than 2 µm, is extracted from the top centimeter of the flask using a laboratory pipette. This fraction is then placed on a glass slide and left to dry for 24 hours.

For certain samples where rapid sedimentation was observed, the clay fraction was extracted immediately after shaking. Once the slides are dry, they are ready for Analysis in a diffractometer, where the normal spectra are obtained. Subsequently, the slides are treated by solvating with ethylene glycol in a vacuum chamber. After this treatment, new spectra are recorded using the diffractometer. Finally, the slides are heated to 500°C for 2 hours, and spectra corresponding to the heat-treated samples are obtained. These three sets of spectra are essential for determining the clay minerals present in the samples.

.

c. Equipment

The instrument used for X-ray diffraction of the samples was a Bruker D8-Advance diffractometer from the Clay, Geochemistry, and Sedimentary Environments Laboratory at the University of Liège.

d. General information on adsorbates: Helianthine

The adsorbate used for this experiment is helianthine, also known as methyl orange or methyl orange. It is a color indicator that turns pink-red in acidic media and yellow-orange in basic media. The main properties of the helianthine used are in line with those of the helianthine used by **Deneche** and **Laouadi in 2020**.

2.2 Methods

a. X-ray diffraction analysis

The objective of this Analysis is to identify the various minerals present in each sample. This technique is employed to ascertain the different mineral phases from the total powder analysis (**Frédéric et *al.*, 2014**) and to qualitatively determine clay constituents (**Robert, 1975**). It is particularly effective for identifying fine fractions, including clay minerals.

Principle

In this process, the powdered sample is subjected to X-ray bombardment. The interaction between X-rays and matter is governed by Maxwell's equations, which describe the coupling between the electric and magnetic fields of the incident wave and the charges of the electrons and nucleus of an atom (**Frédéric et *al.*, 2014**). X-rays are generated by directing an electron beam at a copper anode. The X-rays interact with the single crystals within the powder, which then reflect these X-rays. The reflected rays are detected, and their intensity is recorded at an angle of 2θ. This measurement adheres to Bragg's law, which is expressed by the following formula 1:

$$2.d.\sin\Theta = n.\lambda. \qquad \text{(Formula 1)}$$

Where d is the inter-reticular distance,

Θ is the diffraction angle,

n is an integer relative to the diffraction order

λ is the X-ray wavelength.

This law is illustrated in Figure 1.

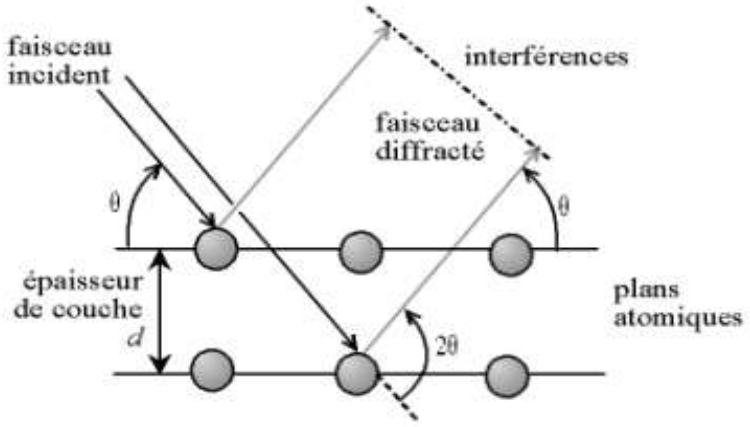

***Figure 1**. Representative diagram of the X-ray diffraction phenomenon (Source: **Yassine, 2016**)*

During Analysis, the sample is rotated by an angle θ, while the counter simultaneously rotates by an angle of 2θ. This is the most commonly employed configuration, although it has the drawback that the powder may become dislodged if θ is set to a high value.

A diffraction spectrum is generated, and EVA software is used to identify the mineral phases present. The spectra plot the number of counts on the ordinate and the basal spacing on the abscissa. Each mineral phase is characterized by distinct peaks corresponding to specific basal spacings (d). For example, a basal spacing of d = 4.47 Å indicates the presence of total clays, while d = 3.33 Å signifies the presence of quartz. This allows for a qualitative assessment of the mineral phases.

After identifying all the mineral phases, a semi-quantitative analysis can be performed to assess the proportion of each mineral phase. The height of each mineral's main peak, reflecting its number of counts, is used for this purpose. The intensity of the main peak for each mineral is determined by multiplying its number of counts by a correction factor (F) specific to each mineral: F = 20 for total clays and F = 1 for quartz. With the intensities of the different mineral phases thus obtained, their proportions in the sample can be calculated.

b. Dye adsorption experiments

Dye adsorption experiments are a valuable aid in determining which clays can be used in water filtration.

Visible spectrometry method

Visible spectrophotometry is employed to determine variations in solution concentration. This technique relies on the ability of certain molecules to absorb light radiation at specific wavelengths.

Principle

Visible spectrophotometry is an analytical method that measures the absorbance or optical density of a solution in accordance with Beer-Lambert's law. This relationship is expressed by the following formula 2:

$$A = \varepsilon \times l \times c \qquad \text{(Formula 2)}$$

With A: absorbance (dimensionless)
ε: Molecular absorption coefficient or molar extinction coefficient (l/mol.cm or cm^2/mol)
l: optical path (cm)
c: concentration of a substance in solution (mol/l)

The following diagram can explain this.

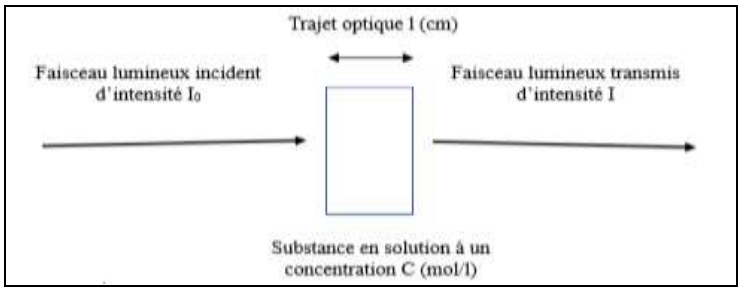

***Figure 2**. Principle of spectrophotometry (Source: **Samake, 2009**)*

In spectrophotometry, two key quantities are used: transmittance (T) and absorbance (A), also referred to as optical density. The following equations relate to these quantities:

$$T = \frac{I}{I_0} \times 100 \qquad \text{(Formula 3)}$$

$$A = log\left(\frac{I}{I_0}\right) \qquad \text{(Formula 4)}$$

The assay can be either direct or indirect (**Samake, 2009**). Although the helianthin solution is colored, this experiment used the indirect calibration range method.

Helianthine calibration curve

A calibration curve is constructed to determine the concentration of helianthin during the experiment. The procedure for preparing this curve involves the following steps:

- A 1 g/L stock solution of helianthin is prepared by dissolving 0.5 g of helianthin powder in 500 mL of water.

- A series of diluted solutions with concentrations ranging from 10 to 60 mg/L is prepared from the stock solution. The required volumes of the stock solution and distilled water for these dilutions are calculated using the following equations:

$$C_i V_i = C_f V_f \quad \text{(Formula 5)}$$

$$V_e = V_f - V_i \quad \text{(Formula 6)}$$

With

C_i: concentration of the stock solution (g/l)
V_i: volume of stock solution required (l)
C_f: concentration of daughter solution (g/l)
V_f: volume of daughter solution (l)
V_e: volume of water required for dilution (l)

***Photo 1**. Helianthine stock and daughter solutions for the calibration curve.*

- The absorbance of the daughter solutions is determined using visible spectrophotometry at a wavelength of 457 nm.

The results are summarized in Table 2 below.

Table 2. Results of spectrophotometric determination of helianthin daughter solutions.

Sample	1	2	3	4	5	6
Concentration	10	20	30	40	50	60
Absorbance	0,166	0,437	0,862	1,209	1,583	1,738

- Plot absorbance versus concentration of methyl orange solution (Figure 3).

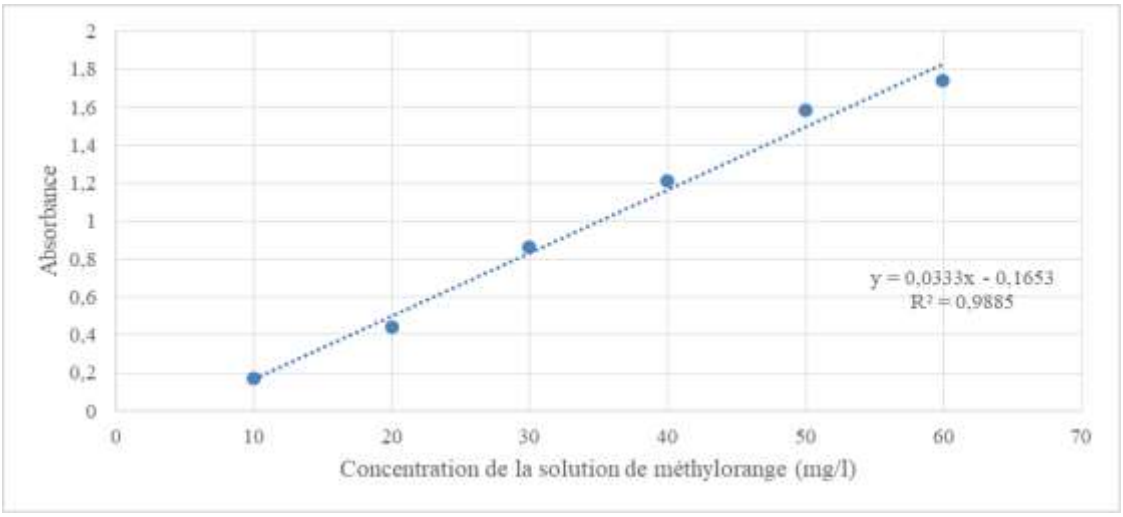

***Figure 3**. Helianthine calibration curve at λ=457nm*

The calibration curve is represented by the equation A = 0.0333C − 0.1653, which is derived from the spectrophotometric absorbance measurements. The curve demonstrates a high correlation coefficient of R^2=0.9885, signifying a robust linear relationship. This linear equation can be used to calculate the concentration of any given solution.

$$C = \frac{A + 0{,}1653}{0{,}0333}$$ (Formula 7)

Adsorption capacity

In a 250 mL beaker, 100 mL of a helianthin solution with an initial concentration C_0 = 60 mg/L is prepared. 1 g of clay, whose adsorption capacity is to be determined, is added to this solution, and the mixture is continuously stirred.

To monitor changes in the helianthin concentration, samples are collected every 10 minutes into test tubes over 50 minutes (see Photo 2). Following this, the clay and solution are allowed to remain in contact for an additional 40 minutes before the final sample is taken.

***Photo 2**. Samples for assay*

Based on the samples' specific surface area, BMLL 001, BMLL 002, BMLL 003, and BMLL 004, along with sample MNDV 003, were selected for the experiment. This selection

aims to elucidate variations in adsorption capacity as influenced by the type of clay and its specific surface area.

c. Phytochemical screening of clay

In addition to the characterization analyses, a phytochemical screening is conducted at the LCM Laboratory in Ampasampito to detect the presence of various chemical families, including saponins, deoxyoses, tannins, and coumarins. Four types of extracts are prepared to test for these chemical families: aqueous extract, hydroethanol extract, chloroform extract, and acid extract. Each extract is then subjected to specific tests to identify the presence of these chemical compounds.

***Photo 3**. Screening in test tubes*

During the test, a fixed volume of an extract is taken in a test tube and reacted with various reagents to determine whether the chemical family is present by precipitation or coloration.

III. Results and Discussion

3.1 Results

a. X-ray diffraction analysis

<u>Analavory samples</u>

Figures 4 and 5 present the X-ray diffraction patterns for clay samples ANLV 001 and ANLV 002, respectively.

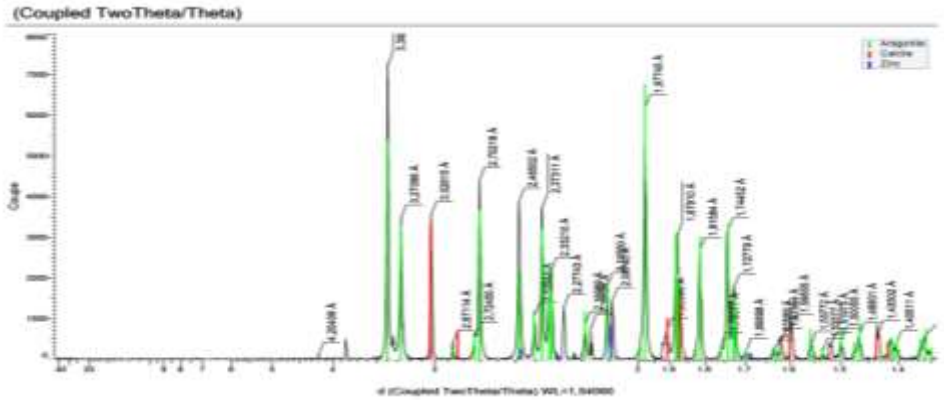

***Figure 4**. X-ray diffractogram of ANLV 001 clay (yellow clay)*

For sample ANLV 001 (yellow clay), the diffraction pattern reveals characteristic lines of aragonite. Additionally, calcite is identified as an associated clay mineral, while zinc is noted as an associated element.

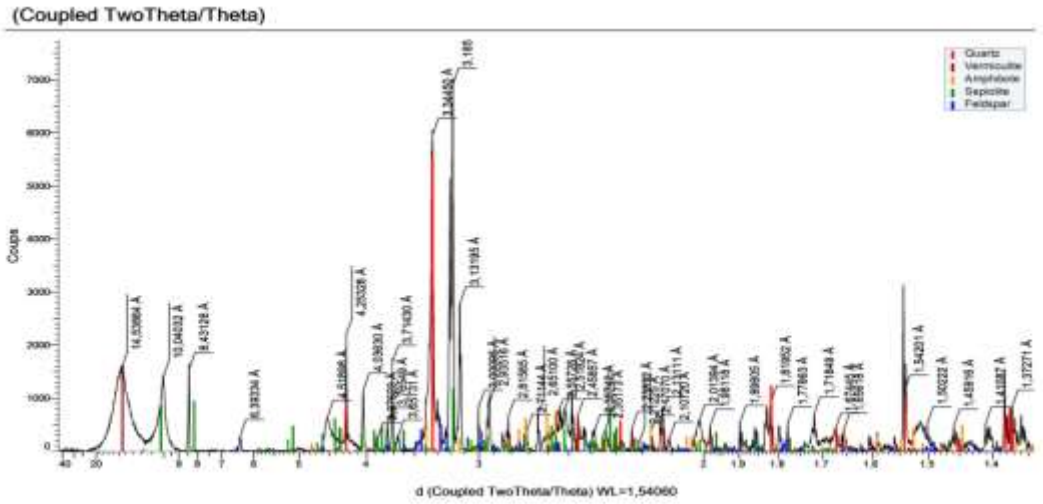

***Figure 5**. X-ray diffractogram of ANLV 002 Clay (Green Clay)*

In sample ANLV 002 (green clay), the diffraction pattern shows characteristic lines of vermiculite, along with the presence of sepiolite and amphibole. Furthermore, quartz and feldspar are identified as associated minerals

Bemololo samples

The X-ray diffraction (XRD) patterns for the Bemololo clay samples BMLL 001, BMLL 002, BMLL 003, and BMLL 004, as depicted in Figures 6, 7, 8, and 9, reveal distinct mineralogical compositions.

These XRD patterns underscore the heterogeneity of the Bemololo clays, each sample exhibiting a unique mineralogical profile. The presence of minerals such as kaolinite, quartz, and muscovite across multiple samples suggests a shared geological origin or similar formation processes. However, the diversity of associated minerals like anatase, hematite, and vermiculite highlights the complexity of these clays, which may influence their potential applications in various industrial and environmental contexts.

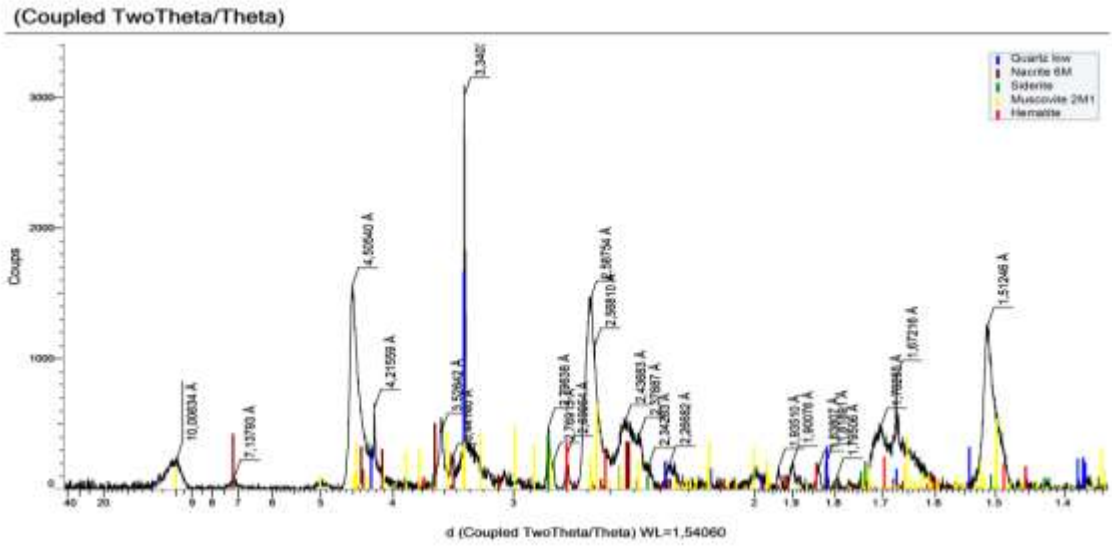

***Figure 6.** BMLL 001 Green clay*

The XRD analysis of BMLL 001 identifies quartz, nacrite, siderite, muscovite, and hematite. The diffraction peaks for quartz, siderite, and hematite are particularly prominent, suggesting these minerals are present in notable quantities alongside nacrite and muscovite (Figure 6).

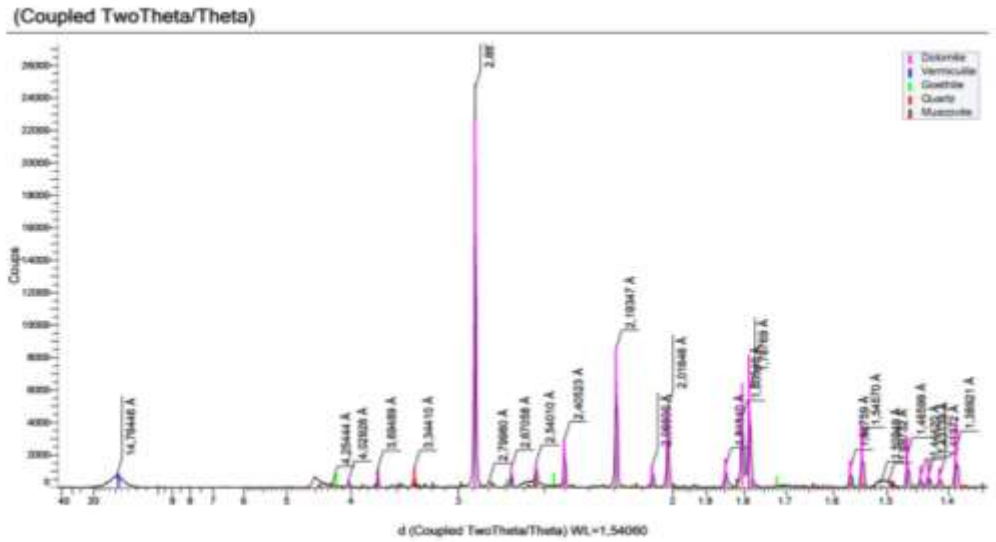

***Figure 7**. BMLL 002 White Clay*

For BMLL 002, the diffraction pattern reveals characteristic lines of vermiculite, indicating its primary composition. Additionally, the corresponding peaks confirm the presence of muscovite, goethite, quartz, and dolomite, reflecting a diverse mineral assemblage within this sample (Figure 7).

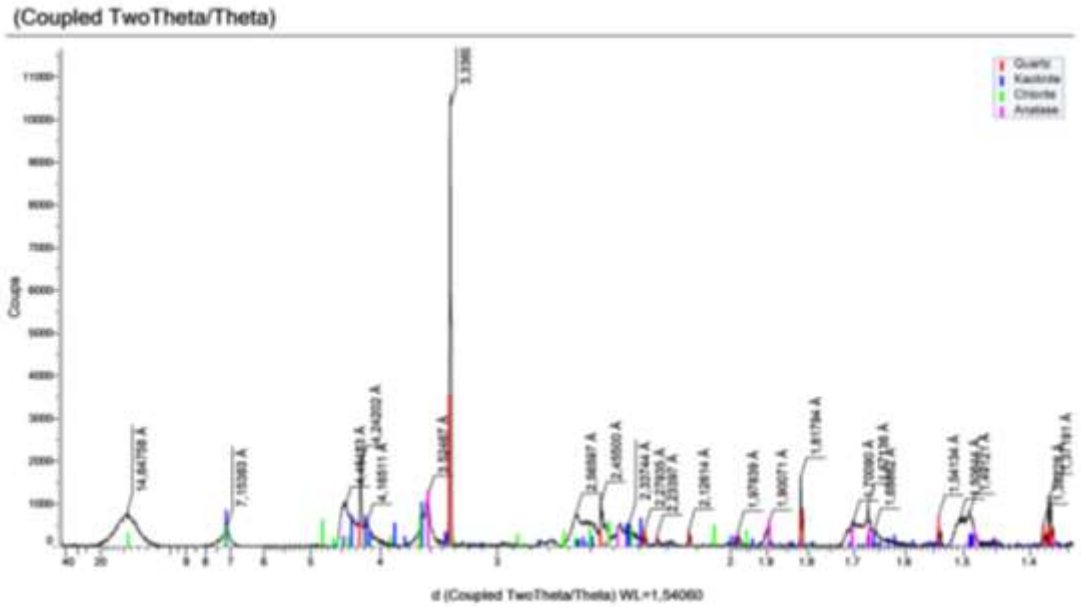

***Figure 8**. BMLL 003 Gray clay*

In BMLL 003, the XRD pattern reveals a composition that includes quartz, kaolinite, chlorite, and anatase. The kaolinite lines are clearly visible, indicating its presence as a major component, while quartz and anatase are also detected as associated phases (Figure 8).

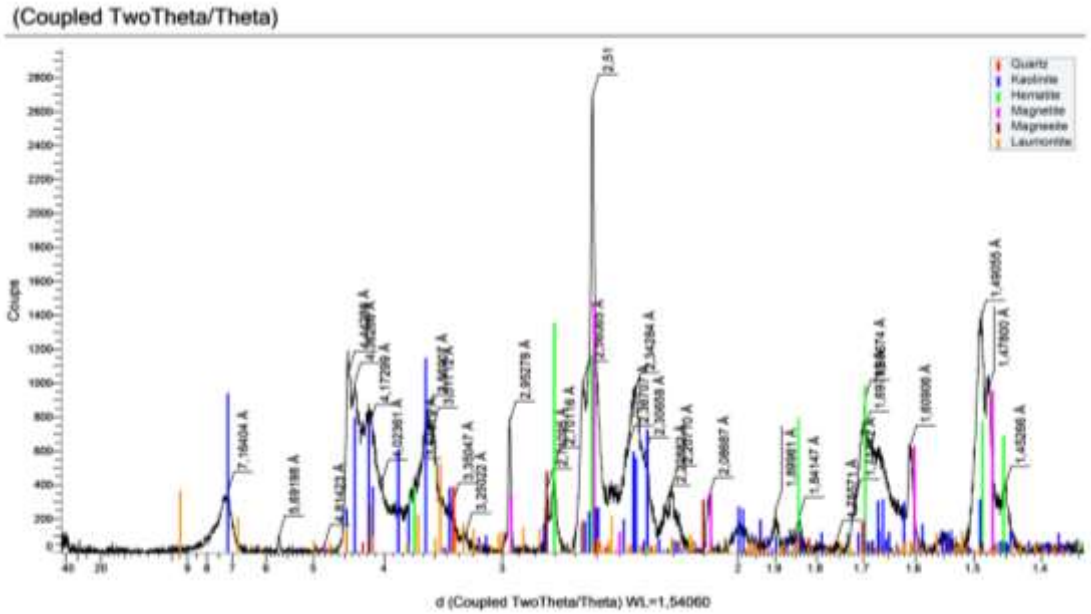

Figure 9. *BMLL 004 Red violet clay*

For BMLL 004, the diffraction pattern indicates the presence of kaolinite as the dominant clay mineral, with additional peaks corresponding to hematite, magnetite, laumontite, magnesite, and quartz. The prominent kaolinite peaks suggest its significant concentration, while the associated minerals confirm the sample's complex mineralogy (Figure 9).

Miandrivazo samples

Figures 10, 11, and 12 present the X-ray diffraction patterns for clay samples MNDV 001, MNDV 002, and MNDV 003, respectively.

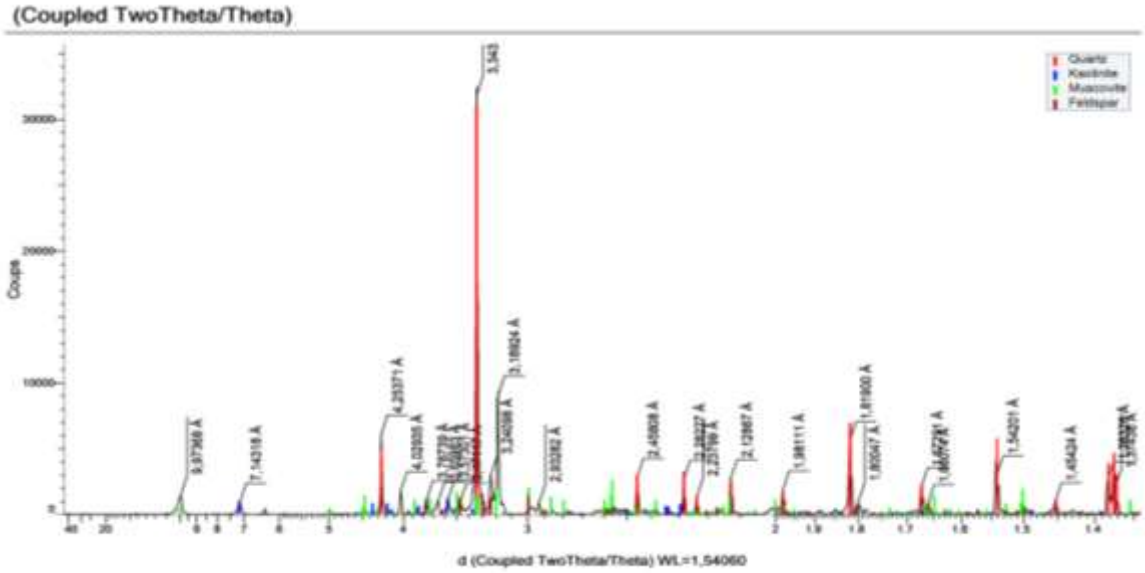

Figure 10*. MNDV 001 Green clay*

X-ray diffraction analysis of MNDV 001 revealed distinctive peaks corresponding to kaolinite, chlorite, and muscovite. Additionally, quartz was identified as an associated mineral phase, highlighting the sample’s diverse mineralogical composition. This mineral

profile suggests MNDV 001 may exhibit specific properties and applications based on the presence of these key minerals.

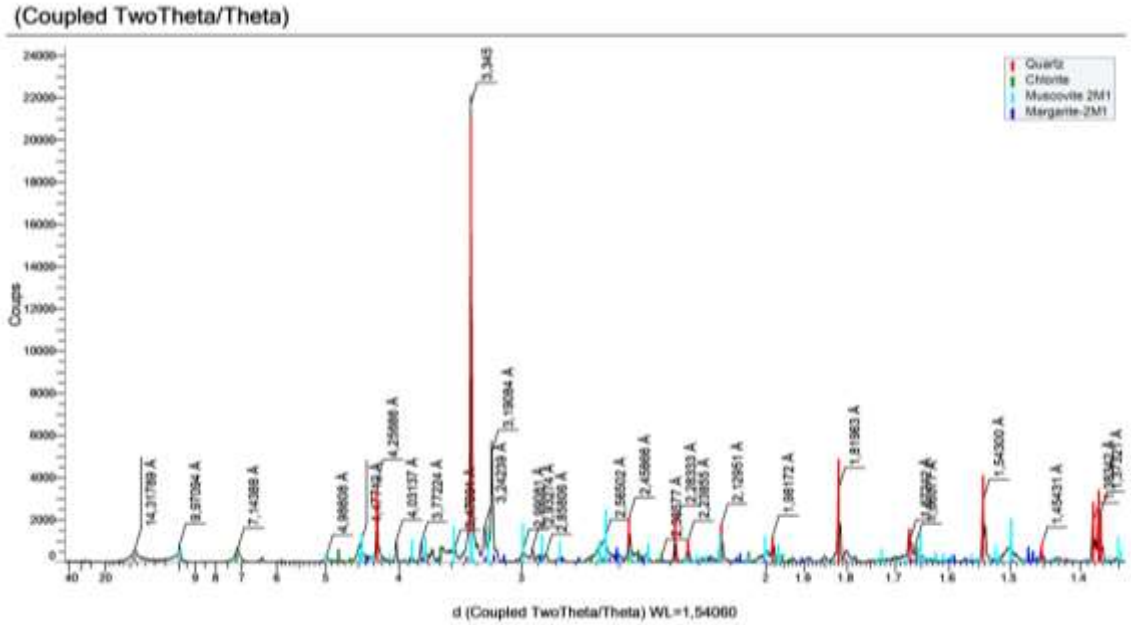

Figure 11. *MNDV 002 Greenish gray clay*

The diffraction pattern for MNDV 002 indicated the presence of quartz, chlorite, muscovite, and margarite. This combination of minerals reflects a complex composition, with each mineral contributing to the sample's overall properties and potential uses in various applications, including those requiring specific mineral interactions.

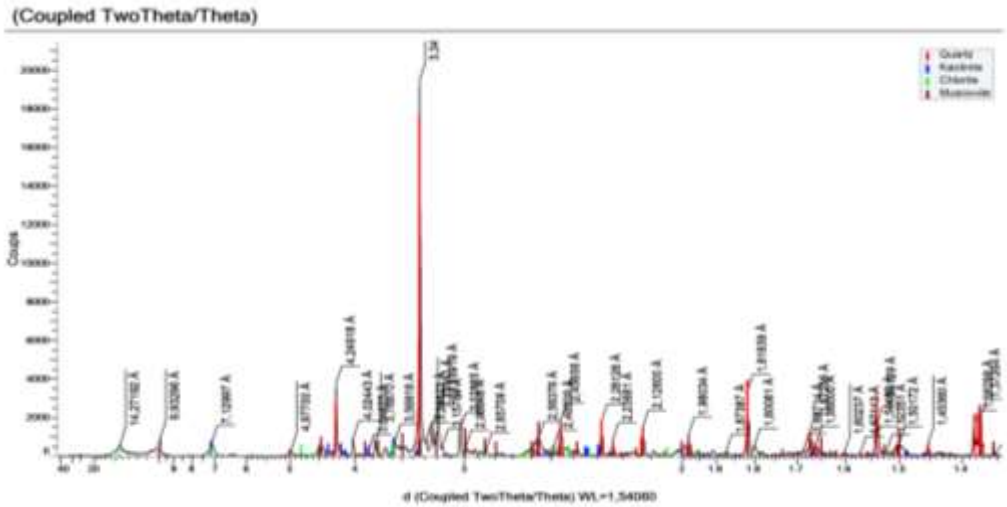

Figure 12. *MNDV 003 Red clay*

Analysis of MNDV 003 showed the presence of quartz, kaolinite, muscovite, and feldspar. The diffraction peaks confirmed these minerals, indicating a varied mineral composition. The combination of kaolinite and feldspar, in particular, suggests potential applications where these minerals' properties are advantageous.

b. Dye adsorption experiments

The results from the dye adsorption experiments, which include absorbance measurements obtained via spectrophotometry, the evolution of helianthin solution

concentration during adsorption, the adsorption capacity q_e of each sample at specific time intervals, and the adsorbate removal rate R, are comprehensively summarized in the respective tables for each sample.

These data have been plotted on representative curves to provide a clearer visualization of the adsorption process. They specifically illustrate the progression of helianthin adsorption at an initial concentration of 60 mg/L.

Adsorption capacity of MNDV 003

Table 3. Adsorption capacity of MNDV 003 towards methyl orange

t (min)	0	10	20	30	40	50	110
A	1,833	1,273	1,218	1,216	1,212	1,059	1,057
C (mg/l)	60	43,192	41,541	41,480	41,360	36,766	36,706
q_e (mg/g)	0	1,681	1,846	1,852	1,864	2,323	2,329
R (%)	0	28,013	30,766	30,866	31,066	38,724	38,824

With T: Time; A: Absorbance, C: Concentration, q_e: Adsorption capacity, and R: Removal rate

Table 3 details the adsorption capacity of MNDV 003 for methyl orange over time. As time progresses, absorbance (A) decreases from an initial value of 1.833 at 0 minutes to 1.057 at 110 minutes, indicating the gradual uptake of methyl orange by the clay. Correspondingly, the concentration (C) of methyl orange decreases from 60 mg/L to 36.706 mg/L over the same period.

The adsorption capacity (q_e) of MNDV 003 increases steadily, starting at 0 mg/g and reaching 2.329 mg/g after 110 minutes, reflecting the clay's growing capacity to adsorb methyl orange. The removal rate (R) similarly rises, beginning at 0% and achieving 38.824% at 110 minutes.

These values indicate that MNDV 003 exhibits significant adsorption potential for methyl orange, with both the adsorption capacity and removal rate improving over time as the clay approaches adsorption equilibrium.

The helianthine concentration curve and the adsorbate uptake versus time curve are then obtained (Figures 13 and 14).

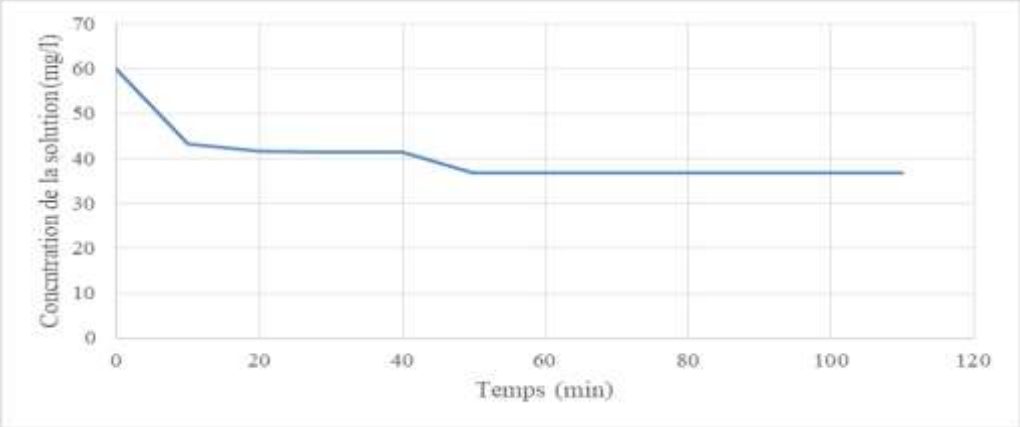

Figure 13*.Concentration curve of the methyl orange solution in contact with MNDV 003 as a function of time*

Figure 13 illustrates the decline in helianthine concentration over time as it interacts with MNDV 003. The curve shows a rapid initial decrease, indicating significant adsorption activity during the early stages. As time progresses, the rate of decline slows, suggesting the approach of equilibrium, where adsorption sites on MNDV 003 become increasingly saturated.

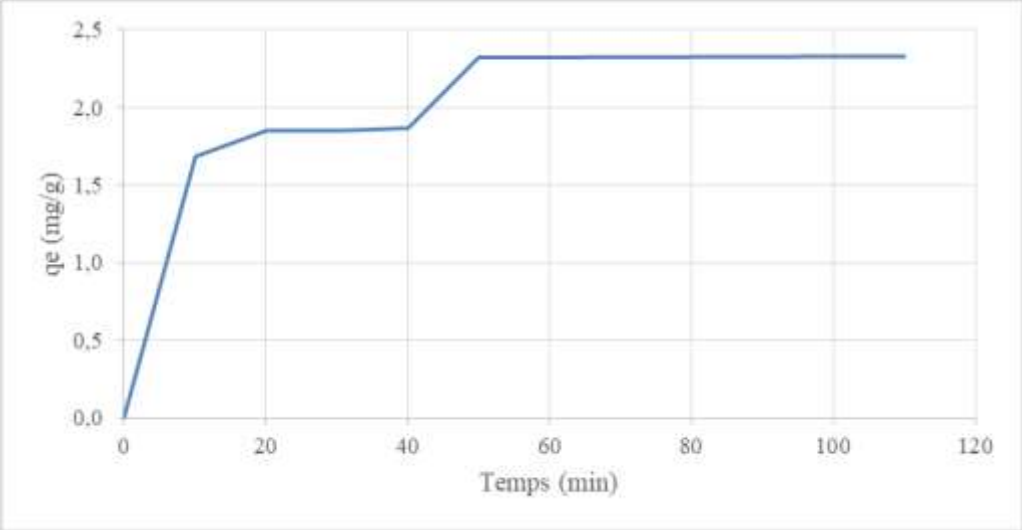

***Figure 14**. Curve showing the amount of adsorbate adsorbed per gram of MNDV 003 as a function of time*

Figure 14 depicts the amount of helianthine adsorbed per gram of MNDV 003 over time. The curve demonstrates a steady increase in adsorption capacity, with a rapid uptake in the initial period followed by a gradual plateau as equilibrium is approached.

Adsorption capacity of BMLL 003

Table 4 Adsorption capacity of BMLL 003 towards methyl orange.

t (min)	**0**	**10**	**20**	**30**	**40**	**54**	**95**
A	1,833	1,195	1,177	1,170	1,137	1,105	0,663
C (mg/l)	60	40,850	40,309	40,099	39,108	38,147	24,874
q_e (mg/g)	0	1,915	1,969	1,990	2,089	2,185	3,513
R (%)	0	31,917	32,818	33,168	34,820	36,421	58,544

Table 4 details the adsorption capacity of BMLL 003 for methyl orange over time. The absorbance (A) decreases from an initial value of 1.833 at 0 minutes to 0.663 after 95 minutes, reflecting the clay's progressive uptake of methyl orange. Correspondingly, the concentration (C) of methyl orange decreases from 60 mg/L to 24.874 mg/L during the same period.

The adsorption capacity (q_e) of BMLL 003 increases steadily, beginning at 0 mg/g and reaching 3.513 mg/g after 95 minutes, indicating an enhanced ability of the clay to adsorb methyl orange. The removal rate (R) similarly rises from 0% to 58.544%, demonstrating the efficiency of BMLL 003 in reducing the concentration of methyl orange in solution.

The adsorption capacity of BMLL 003 is then plotted against time.

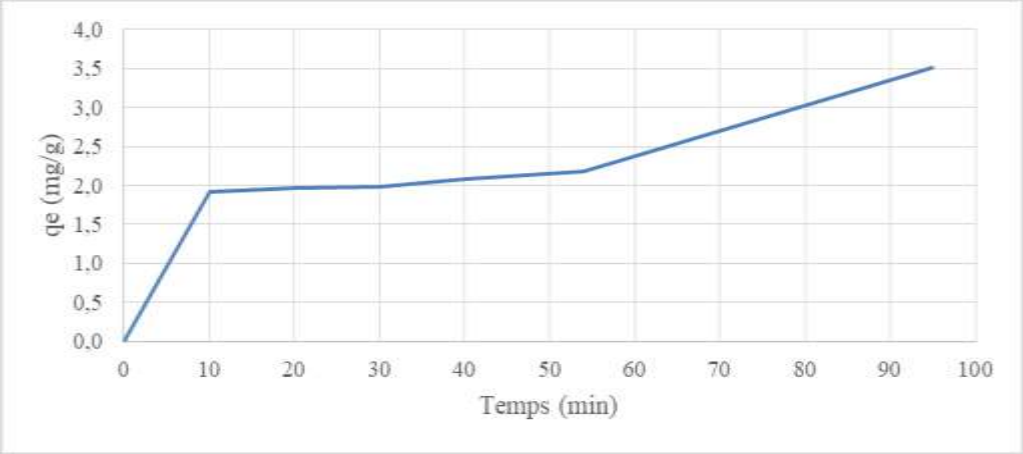

***Figure 15**. Quantity of adsorbate adsorbed per gram of BMLL 003 versus time*

Figure 15 illustrates the adsorption capacity (q_e) of BMLL 003 as a function of time, showing a consistent increase in adsorbate uptake, with a notable acceleration as the contact time extends, suggesting that BMLL 003 continues to adsorb effectively even after prolonged exposure.

Adsorption capacity of BMLL 004

Table 5: Adsorption capacity of BMLL 004 towards methyl orange.

t (min)	**0**	**10**	**20**	**30**	**40**	**50**	**110**
A	1,833	1,729	1,515	1,466	1,451	1,418	1,404
C (mg/l)	60	56,886	50,459	48,988	48,538	47,547	47,126
q_e (mg/g)	0	0,311	0,954	1,101	1,146	1,245	1,287
R (%)	0	5,190	15,901	18,353	19,104	20,756	21,456

Table 5 presents the adsorption capacity of BMLL 004 for methyl orange over time. Initially, the absorbance (A) drops from 1.833 to 1.404 after 110 minutes, reflecting the gradual adsorption process. The corresponding concentration (C) of methyl orange decreases from 60 mg/L to 47.126 mg/L.

The adsorption capacity (q_e) of BMLL 004 increases progressively, starting at 0 mg/g and reaching 1.287 mg/g by the end of the 110-minute period, demonstrating the clay's ability to adsorb methyl orange over time. The removal rate (R) also shows a consistent increase, from 0% to 21.456%, indicating the efficiency of BMLL 004 in reducing the concentration of methyl orange in solution.

Figure 16 illustrates the curve showing the variation in BMLL 004's adsorption capacity as a function of time.

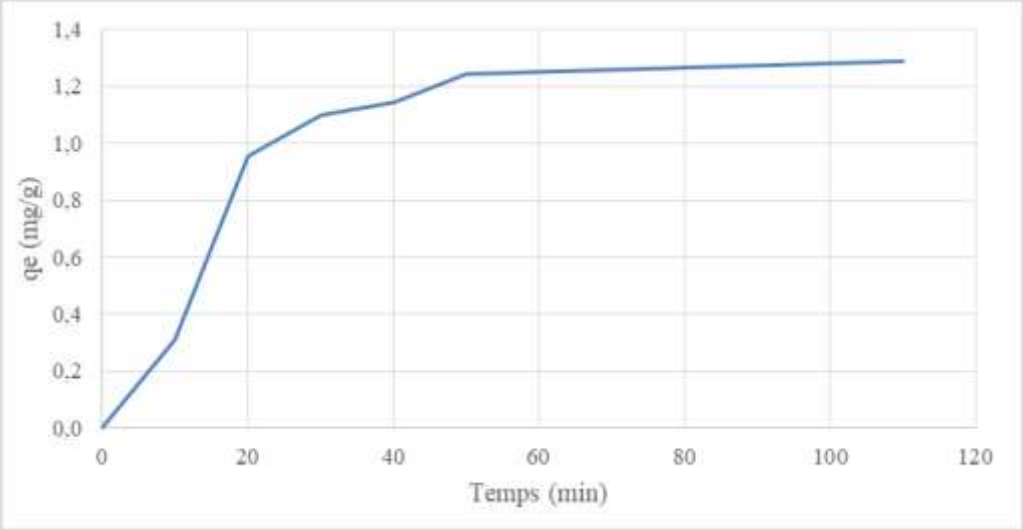

***Figure 16**. Curve showing the amount of adsorbate adsorbed per gram of BMLL 004 as a function of time*

Figure 16 visually represents the variation in BMLL 004's adsorption capacity as a function of time. The curve shows a steady rise in adsorbate uptake, with a notable increase in adsorption capacity as the contact time extends. This suggests that BMLL 004 continues to adsorb methyl orange effectively, albeit at a slower rate as equilibrium approaches.

Adsorption capacity of BMLL 002

Table 6: Adsorption capacity of BMLL 002 towards methyl orange.

t (min)	**0**	**10**	**20**	**30**	**40**	**55**	**90**
A	1,833	0,866	0,650	0,632	0,629	0,605	0,507
C (mg/l)	60	30,970	24,483	23,943	23,853	23,132	20,189
q_e (mg/g)	0	2,903	3,552	3,606	3,615	3,687	3,981
R (%)	0	48,383	59,194	60,095	60,245	61,446	66,351

Table 6 details the adsorption capacity of BMLL 002 for methyl orange, highlighting a significant reduction in absorbance (A) from 1.833 to 0.507 over a 90-minute period. This reduction corresponds to a marked decrease in methyl orange concentration (C) from 60 mg/L to 20.189 mg/L.

The adsorption capacity (q_e) of BMLL 002 continuously increases, beginning at 0 mg/g and reaching 3.981 mg/g by the end of the experiment. This progressive rise indicates the clay's effectiveness in adsorbing methyl orange from the solution. Similarly, the removal rate (R) improves steadily, from 0% to 66.351%, reflecting the clay's efficiency in reducing the concentration of the dye.

Figure 17 shows the evolution of the adsorption capacity of BMLL 002 towards methyl orange as a function of time.

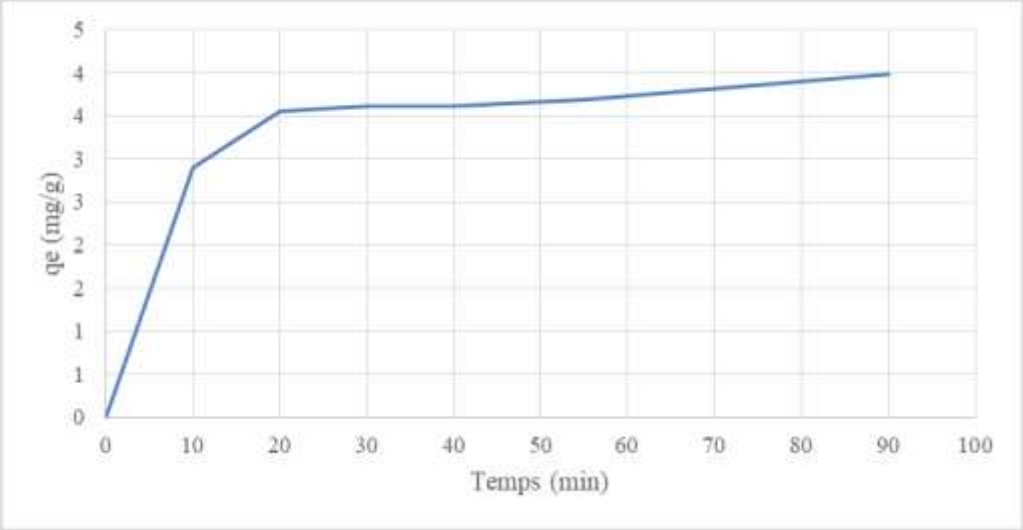

Figure 17*.Curve showing the amount of adsorbate adsorbed per gram of BMLL 002 as a function of time*

Figure 17 illustrates the relationship between contact time and adsorption capacity. The curve demonstrates a rapid initial increase in adsorbate uptake, followed by a gradual approach to equilibrium. The sustained increase in adsorption capacity (q_e) throughout the time period suggests that BMLL 002 exhibits strong adsorption capabilities, efficiently capturing methyl orange molecules as time progresses.

Adsorption capacity of BMLL 001

Table 7: Adsorption capacity of BMLL 001 towards methyl orange.

T (min)	**0**	**10**	**20**	**30**	**40**	**50**	**110**
A	1,833	1,761	1,730	1,724	1,702	1,651	1,444
C (mg/l)	60	57,847	56,916	56,736	56,075	54,544	48,327
q_e (mg/g)	0	0,215	0,308	0,326	0,392	0,546	1,167
R (%)	0	3,589	5,140	5,440	6,542	9,094	19,454

Table 7 outlines the adsorption capacity of BMLL 001 towards methyl orange. It indicates a gradual decrease in absorbance (A) from 1.833 to 1.444 over 110 minutes. Correspondingly, the concentration of methyl orange (C) drops from 60 mg/L to 48.327 mg/L.

The adsorption capacity (q_e) increases steadily, starting from 0 mg/g and reaching 1.167 mg/g, demonstrating a progressive uptake of the dye by the clay. The removal rate (R) also shows a consistent rise, from 0% to 19.454%, reflecting the clay's moderate efficiency in removing methyl orange from the solution.

The BMLL 001 adsorption capacity curve is then plotted against time.

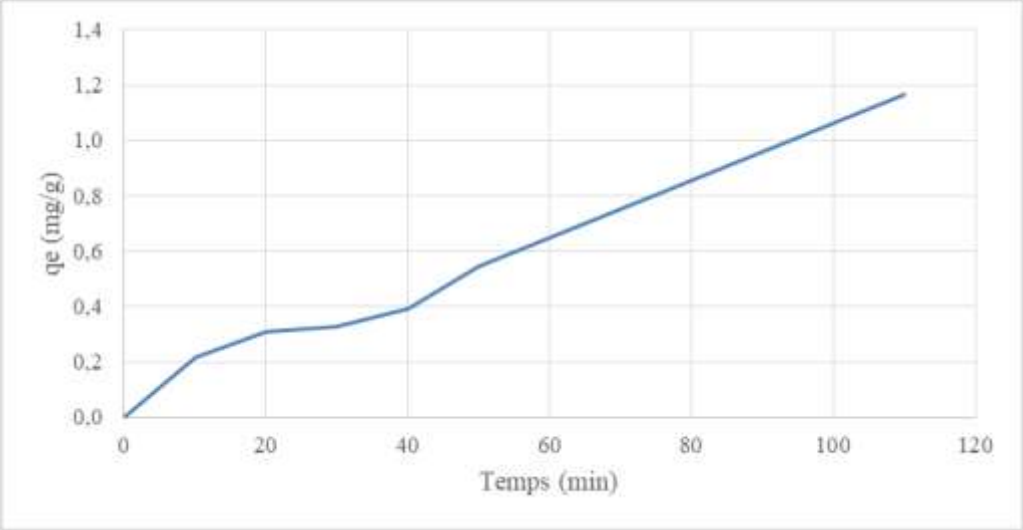

Figure 18. *Curve of adsorbate quantity adsorbed per gram of BMLL 001 as a function of time*

Figure 18 presents the curve of adsorbate quantity adsorbed per gram of BMLL 001 over time, highlighting a slow yet continuous increase in adsorption capacity. This suggests that while BMLL 001 is effective, it exhibits a slower adsorption rate compared to other samples.

The diagram in Figure 19 shows the rate of methyl orange removal by each sample at a contact time of 95 minutes to better compare the adsorption capacity of these five clays.

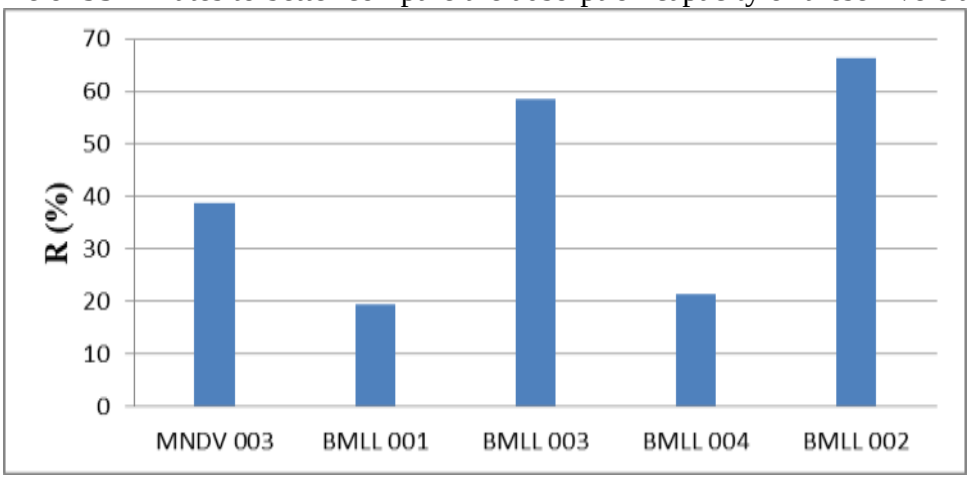

Figure 19*. Diagram of methyl orange removal rate by the five clay samples at 95min contact time*

Figure 19 further compares the removal rates of methyl orange by five different clay samples at a contact time of 95 minutes, offering a visual representation of the varying efficiencies of each clay in adsorbing the dye. BMLL 001, though effective, demonstrates a lower adsorption capacity relative to the other samples in this comparison.

c. Analysis by photochemical screening

The results obtained are summarized in Table 8 below.

Table 8. Phytochemical screening results for clays.

Chemical family	MNDV 003	MNDV 001	MNDV 002	BMLL 001	BMLL 003	BMLL 004	BMLL 002	ANLV 002	ANLV 001
Saponosides	-	-	-	-	-	-	-	-	-
Deoxyose	-	-	-	-	-	+	-	-	-
Tanin	-	-	-	-	-	-	+	+	+
Coumarin	-	-	-	-	-	-	-	-	-

A positive result indicates the presence of the chemical family, while a negative result indicates its absence.

Table 8 reveals that among the clays analyzed, only deoxyose and tannin were detected. Deoxyose was exclusively found in BMLL 004, while tannin was present in BMLL 002, ANLV 002, and ANLV 001.

3.2 Discussion

a. X-ray diffraction analysis

- The clay fraction in sample ANLV 001 predominantly comprises aragonite and calcite.
- The composition of ANLV 002 clay is primarily vermiculite, a mineral belonging to the TOT clay family. This finding aligns with the characterization by **Valášková** and **Martynkova** (**2012**), who identified vermiculite as a magnesium-rich, volcanic-origin clay, consistent with the properties observed in ANLV 002.
- BMLL 004 clay is characterized by the presence of kaolinite, classifying it within the TO clay family.
- BMLL 003 is a composite clay sample consisting of kaolinite, which is part of the TO family, and chlorite, which belongs to the TOTO family.
- The BMLL 001 clay sample is predominantly muscovite, categorized under the TOT structural group.
- BMLL 002 clay is a mixture of vermiculite, sepiolite, and amphibole, with vermiculite belonging to the TOT clay family.
- MNDV 001 is a complex clay sample containing kaolinite (TO family), muscovite (TOT family), and chlorite (TOTO family).
- The MNDV 002 clay sample is composed of chlorite and muscovite, with chlorite falling under the TOTO family and muscovite under the TOT family.
- MNDV 003 is a blend of kaolinite and muscovite.

Green-colored clay samples have been identified as containing TOT-type clays. A significant number of samples from Bémololo (BMLL) and Miandrivazo (MNDV) exhibit the presence of kaolinite and muscovite. The elevated mass percentage of calcium oxide (CaO) in these samples is indicative of calcite, as noted by **Qlihaa et *al.*** (**2016**). Specifically, the physicochemical Analysis by **Ramahandry et *al.*** (**2024**) revealed that ANLV 001 contains 35.25% CaO, confirming the predominance of calcite in this sample. Additionally, the high levels of silica and aluminum suggest the presence of kaolinite (**Qlihaa et *al.*, 2016**), which is corroborated by the chemical Analysis of MNDV 001, showing 90.00% SiO_2 and 5.58% Al_2O_3 (**Ramahandry et *al.*, 2024**), thus affirming that MNDV 001 is primarily composed of kaolinite.

b. Dye adsorption experiments

Figure 14 illustrates that the adsorption capacity of MNDV 003 for methyl orange increases progressively with time. This trend can be attributed to the gradual diffusion of methyl orange molecules toward the available adsorption sites until equilibrium is achieved,

where all sites are fully occupied. At equilibrium, reached at t = 50 minutes, there is no significant change in the solution's concentration, and consequently, the amount adsorbed stabilizes. The maximum adsorption capacity of MNDV 003 is 2.32 mg/g, corresponding to 38.8% of the initial adsorbate.

After 95 minutes, the removal rate increases to 58.54%. However, as depicted in Figure 15, equilibrium has yet to be fully established, as the amount of adsorbate bound continues to vary with time.

The majority of helianthine adsorption occurs within the first 20 minutes, with equilibrium achieved at t = 50 minutes, resulting in an elimination rate of R = 20.75% (Figure 16).

Figure 17 demonstrates that helianthine adsorption on BMLL 002 is particularly rapid during the initial 10 minutes, followed by a slower increase in adsorption capacity with prolonged contact time. This behavior is likely due to the abundance of active sites available at the onset of adsorption. Although the adsorption rate decelerates, equilibrium has not yet been reached. After 90 minutes of contact, the elimination rate reaches 66.35%.

The adsorption of methyl orange by BMLL 001 is notably slower compared to the other samples (Figure 18). The adsorption capacity increases gradually, reaching only 1.167 mg of methyl orange per gram of BMLL 001 after 110 minutes of contact. The slow rate of this process suggests that the adsorption of methyl orange by BMLL 001 may be governed by chemical adsorption.

Across the five samples studied, removal rates ranged from 19% to 66% at a contact time of 95 minutes. During this period, BMLL 002 exhibited the highest adsorption capacity, while BMLL 001 showed the lowest. Only BMLL 004 and MNDV 003 achieved equilibrium within this time frame, indicating that methyl orange adsorption by the other clays would likely continue with increased contact time.

Considering the specific surface area of these samples, it was hypothesized that BMLL 001 and BMLL 004, with their larger active sites, would exhibit higher elimination rates. However, the results contradict this hypothesis, suggesting that the high absorbency of BMLL 001 and BMLL 004 is associated with lower absorbency.

c. Photochemical screening analysis

The phytochemical screening results presented in Table 8 indicate a limited presence of specific chemical families across the clays studied. Notably, deoxyose was detected solely in BMLL 004, signifying its unique composition compared to the other samples. Tannin was identified in three samples: BMLL 002, ANLV 002, and ANLV 001, highlighting a commonality in their chemical profiles. However, no saponosides or coumarins were detected in any of the clays, suggesting that these particular chemical families are absent across the entire sample set. The selective presence of deoxyose and tannin in specific clays underscores the potential variability in their phytochemical compositions, which could influence their functional properties and applications. This differentiation may be pertinent in the context of material selection for processes that rely on specific chemical attributes.

As can be seen from Table 8, only deoxyose and tannin are present in the clays studied. Only BMLL 004 contains deoxyose, and BMLL 002, ANLV 002 and ANLV 001 contain tannin.

IV. Conclusion

X-ray diffraction analysis identified the mineral phases within the clay samples, revealing distinct compositions for each. ANLV 001 was found to contain aragonite, while the presence of vermiculite characterizes ANLV 002. BMLL 001 is primarily composed of muscovite, and BMLL 002 includes a mixture of vermiculite, sepiolite, and amphibole.

BMLL 003 consists of kaolinite and chlorite, and BMLL 004 contains kaolinite as well. MNDV 001 comprises kaolinite, muscovite, and chlorite, while MNDV 002 and MNDV 003 include chlorite and muscovite, and kaolinite and muscovite, respectively. This detailed mineralogical characterization was crucial in assessing the potential applications of these clays.

The adsorption study on methyl orange demonstrated that among the five clay samples, BMLL 003 exhibited the highest adsorption capacity, whereas BMLL 001 had the lowest, within a contact time of 110 minutes. Notably, BMLL 002 achieved a removal rate of 66% after 90 minutes. These findings suggest that the clays have significant potential for use in water treatment processes, particularly for the removal of unwanted dyes or ions.

Given their mineralogical properties and structural characteristics, these clays also have broad applications, including in cosmetics, where they play a vital role.

Acknowledgments

We want to express our sincere gratitude to the staff of the Laboratory of LCM (Laboratory of Chemical and Microbiology) Ampasampito, the Laboratory of Mineral at ESPA Vontovorona, and Laboratoire Argiles, Géochimie et Environnements sedimentary de l'Université de Liège for their collaborations.

References

Abdoulkader, A. B., Elmi, M. A., Abdillahi, H. S., & Mohamed, D. H. (2021). Assessment of physicochemical properties of clays for pharmaceutical and cosmetic applications. Journal of Applied Clay Science, 205, 106039.

Bergaya, F., & Lagaly, G. (2013). Handbook of clay science (Vol. 5). Elsevier.

Deneche, C. E., Laouadi, S. and Allama F. (2020). Evaluation of the adsorbent capacity of local clay. Université Oum El Bouaghi. https://hdl.handle.net/123456789/10728.fr .

Frédéric S., Jean L., Jean-Marc C. (2014). X-ray diffraction: a powerful technique for solving certain industrial and technological problems. Centre de Recherches de l'Industrie Belge de la Céramique, Avenue du Gouverneur Emile Cornez, 4, 7000 MONS.

Gravereau P. (2012). Introduction to the practice of X-ray powder diffraction. Bordeaux Institute of Condensed Matter Chemistry - CNRS, University of Bordeaux.

Grim, R. E. (1968). Clay mineralogy. McGraw-Hill.

Moore, D. M., & Reynolds, R. C. (1989). X-ray diffraction and the identification and Analysis of clay minerals. Oxford University Press.

Qlihaa A., Dhimni S., Melrhaka F., Hajjaji N., Srhiri A. (2016). Physico-chemical characterization of Morrocan clay. Materials, Electrochemistry and Environment Laboratory. Faculté des Sciences, Université Ibn Tofail de Kénitra, BP 133, 14000 Kénitra, Maroc. J. Mater. Environ. Sci. 7 (5) (2016) 1741-1750, ISSN: 2028-2508, CODEN: JMESCN.

Ramahandry J.E, Robijaona Rahelivololoniaina B.,, Randriantsimbazafy A., Razafindramanga A.W., Letsara R., Razafindrakoto F.N.R., Koto-te-Nyiwa Ngbolua,

Mandimbiharison A. (2024). Physico-Chemical and Mineralogical Characterization of Analavory, Bemololo and Miandrivazo Clays. Budapest International Research in Exact Sciences (BirEx) Journal Volume 6, No 2 April 2024, Page: 104-118 e-ISSN: 2655-7827 (Online), p-ISSN: 2655-7835 (Print) www.bircu-journal.com/index.php/birex email: birex.journal@gmail.com.

Robert M. (1975). Principles of qualitative determination of clay minerals using X-rays. Annales Agronomiques, 26, 363-399.

Samake D., 2009. Treatment of tannery wastewater using clay-based materials. Sciences de la terre. Université Joseph-Fourier - Grenoble I, 2008. François. tel-00360969 https://tel.archives-ouverts.fr/tel-00360969 .

Valášková M., Martynkova G. S. (2012). Vermiculite: structural properties and examples of The use. Clay minerals in nature characterization, modification, and application, InTech, p 209-238.

Yassine B. (2016). Physicochemical characterization of Moroccan clays: application of the adsorption of arsenic and cationic dyes in aqueous solution. Other. COMUE

Université Côte d'Azur (2015 - 2019); Université Abdelmalek Essaâdi (Tétouan, Morocco). French. NNT: 2016AZUR4081. Tel-01452518.